OPEN ACCESS
Journal of Innovative Optical Health Sciences
Vol. 16, No. 2 (2023) 2244001 (13 pages)

DOI: 10.1142/S1793545822440011

World Scientific
www.worldscientific.com

Label-free breast cancer detection and classification by convolutional neural network-based on exosomes surface-enhanced raman scattering

Xiao Ma*, Honglian Xiong†, Jinhao Guo*, Zhiming Liu*, Yaru Han*, Mingdi Liu†, Yanxian Guo*, Mingyi Wang†, Huiqing Zhong*,‡,¶ and Zhouyi Guo*,§,¶

*MOE Key Laboratory of Laser Life Science
& Institute of Laser Life Science
SATCM Third Grade Laboratory of
Chinese Medicine and Photonics Technology
& Guangdong Provincial Key Laboratory of Laser Life Science
Guangzhou Key Laboratory of
Spectral Analysis and Functional Probes
College of Biophotonics
South China Normal University
Guangzhou 510631, P. R. China

†Department of Physics and Optoelectronic Engineering
Foshan University, Guangdong 528011, P. R. China
‡zhonghq@scnu.edu.cn
§ann@scnu.edu.cn

Received 20 February 2022
Accepted 4 May 2022
Published 12 October 2022

Because the breast cancer is an important factor that threatens women's lives and health, early diagnosis is helpful for disease screening and a good prognosis. Exosomes are nanovesicles, secreted from cells and other body fluids, which can reflect the genetic and phenotypic status of parental cells. Compared with other methods for early diagnosis of cancer (such as circulating tumor cells (CTCs) and circulating tumor DNA), exosomes have a richer number and stronger biological stability, and have great potential in early diagnosis. Thus, it has been proposed as promising biomarkers for diagnosis of early-stage cancer. However, distinguishing different exosomes remain is a major biomedical challenge. In this paper, we used predictive Convolutional Neural model to detect and analyze exosomes of normal and cancer cells with surface-enhanced Raman scattering (SERS). As a result, it can be seen from the SERS spectra that the exosomes of MCF-7, MDA-MB-231 and MCF-10A cells have similar peaks (939, 1145 and 1380 cm^{-1}). Based on this dataset, the predictive model can achieve 95% accuracy. Compared with principal component analysis (PCA), the trained CNN can classify exosomes from different breast cancer

¶Corresponding authors.

cells with a superior performance. The results indicate that using the sensitivity of Raman detection and exosomes stable presence in the *incubation period* of cancer cells, SERS detection combined with CNN screening may be used for the early diagnosis of breast cancer in the future.

Keywords: Exosomes; surface-enhanced Raman scattering (SERS); breast cancer; convolutional neural model; label-free.

1. Introduction

In the Global Cancer Statistics 2020, female breast cancer has surpassed lung cancer as the most common cancer for the first time, with an estimated 2.3 million new cases (11.7%), and its mortality rate has risen to 6.9% of global cancers. The breast cancer is the most commonly diagnosed cancer among women and the reason resulting to cancer deaths. This alarming number is expected to rise continually in 2040.[1] In cancer detection, there are many biometric methods including immunoassays (e.g., immunomagnetic separation, ELISA), genetic identification (e.g., RFLP, FISH, real-time PCR), proteomics and mass spectrometry, etc. However, these techniques have some disadvantages. For example, classical cytogenetic analysis requires metaphase preparation of available tumor cells and FISH assay is usually limited by classical probes targeting one or two candidate genes.[2] The current detection methods for breast cancer mainly include breast color ultrasound, mammography, breast MRI, digital breast tomosynthesis (DBT), fine-needle aspiration pathology examination and pathological examination after breast lumpectomy.[3–5] Unfortunately, these methods may cause discomfort, over diagnosis and false positive results that are usually accompanied by patient distress and anxiety.[6] In addition, the image-based diagnostic tools are also expensive, which may have different performance and quality in each place, and may not be applicable to all people, especially those living in rural areas or remote areas.[7] Therefore, it is particularly important to develop an efficient, highly sensitive, easy-to-operate, non-destructive and highly accurate detection method.

Exosomes are tiny vesicles with a lipid bilayer membrane structure of 30–200 nm in size.[8] It was first discovered in mammalian reticulocytes (immature red blood cells) by Stahl *et al.*[9] and Johnstone *et al.*[10] in 1983, and was further called *exosomes* by Johnstone group in 1987.[11] Initial research reported that exosomes can only be secreted by specialized cells, such as dendritic cells and reticulocytes, but later studies have shown that it can be secreted by most cells, including normal cells and cancer cells.[12–15] Then it was found that exosomes existed in almost all body fluids,[16] including blood, breast milk, urine, cerebrospinal fluid, tears, *etc.*[17–21] They mainly contain nucleic acids (mRNA, miRNA, lncRNA and DNA), proteins and lipids,[22] among which lipids and proteins are the main components. Abnormal cells and diseased organs produce more exosomes compared with normal cells or organs. The total number of exosomes in the blood of each normal person is about 2×10^{15} particles, while the number of exosomes in tumor patients can be as much as 4×10^{15} particles.[23,24] The reason for this phenomenon may be that abnormal cells secreted too much exosomes to inhibit the secretion of exosomes by normal cells.[25] Compared to circulating tumor cells (CTCs), larger amounts of exosomes can be released into the circulatory system in the case of cancer. Because of the high abundance of exosomes in the body and good stability in body fluids (especially blood), exosomes are considered to be a reliable and powerful source of circulating cancer biomarkers.[26] Exosomes reflect the genetic and phenotypic status of their parental cells to a large extent, so they can be used as liquid biopsy materials for many diseases and medical diagnosis.[27]

The Raman scattering effect is an inelastic scattering caused by molecular vibration and lattice vibration. The phenomenon was observed in liquid by C. V. Raman in 1928.[28] With the advantage of non-destructive measurement, Raman spectroscopy can fingerprint specific chemical groups, and does not require special sample preparation steps. In addition, traditional infrared spectroscopy detection methods are susceptible to background interference from aqueous solutions, but the Raman spectroscopy of water is weak. Therefore, Raman spectroscopy is an ideal analytical method for biological samples. However, most samples, especially

biological samples, have weak Raman scattering intensity, which to some extent hinders the application of this technology in certain fields. Surface-enhanced Raman scattering (SERS) can enhance Raman signals from small molecules close to the metal surface through electromagnetic and chemical mechanisms.[29,30] Molecules adsorbing on the surface of rough metal or metal sol particles can obtain a stronger (some increase several orders of magnitude) signal than ordinary Raman scattering.[31,32] In addition, the signal can be acquired in a short time (1 s or faster per spectrum). These characteristics make SERS popular in biological detection and widely used in cancer detection, including the detection of biomarkers in body fluids.[33]

Because of high efficiency, high sensitivity and simplicity, SERS has great clinical application potential in discovering the tumorous exosomes. For example, Tirinato *et al.*[34] used a combined biophotonic device of microstructures, super-hydrophobic surfaces (SHSs) and SERS to analyze exosomes from healthy and tumor of colon cell lines. Based on the remarkable water-resistant capacity, SHSs can concentrate the diluted solution, makes small molecules gather in a very small area and captures the inside analytes. Thus, it can not only increase density, but also reach the detection limit. Recently, it is reported that a SERS substrate of the nanobowl coated with silver film could capture and analyze exosomes. As the small size of the nanobowl, it can be captured by a single bowl and measured by a focused beam. So, several exosomes can be analyzed at once. Exosomes are gathered in sub-micron nanobowl, their signal are generated from the narrow space near the plasma surface, which can provide biochemical analysis of intact and ruptured exosomes.[35] Stremersch *et al.*[36] deposited a gold nanoparticle-based shell on the surface of exosomes derived from cancer cells and healthy cells, which can not only enhance Raman signals, but also maintain a colloidal suspension of individual vesicles. This nanocoating can record SERS spectra from a single vesicle. Even in the same mixture, vesicles from different sources can be distinguished by this method with partial least square discriminant analysis. In addition, a study reported that deep learning methods (Architecture of the Resnet-based deep learning model) combined the SERS to explore the characteristics of exosomes of normal and lung cancer cell lines, then find the similarities of human plasma exosomes without collecting a large number of exosomes.[37] Recently, Li *et al.*[38] proposed a magnetic SERS platform and combined with PCA to distinguish exosomes of breast cancer cells, and breast cancer patients from healthy people. The results are shown that this method can simplify capture exosomes and distinguish cancer from normal, which can avoid exosomes losing and destruction caused by multiple washing and magnetic separation steps after capture.

Deep Learning is a new research direction in the field of computer learning. Specially, convolutional neural network (CNN) has shown promising results in feature extraction and learning.[39] The connection mode between neurons in the deep neural network is similar to the animal visual cortex organization, which includes a learning method of multi-level nonlinear transformation levels. As one of the classic structures, CNN has its characteristics such as local connection, translation invariance, weight sharing, multi-layer structure and pooling operation, with which CNN can effectively and easily train and optimize. Some researchers used CNN to analyze spectroscopic signal including Raman spectroscopy. In biological samples, CNN has been applied to classify exosomes of normal and lung cancer cell lines.[40–44] Generally, CNN can automatically learn data features through multi-layer nonlinear transformations, and its deep structure makes it have strong expression and learning capabilities.[45]

This paper reports a method of combining SERS with CNN to detect exosomes from normal and breast cancer cells. Compared to traditional methods (e.g., PCA), CNN can analyze spectra after simple processing (such as data baseline leveling, normalization, etc.).[40] In this experiment, we isolated exosomes from cell culture supernatant by ultracentrifugation, then mixed with laboratory-synthesized gold nanoparticles (AuNPs). After drying, SERS signals of exosomes were acquired. Spectral data sets of exosomes from different cell lines will be used to train the CNN model to extract different SERS signal characteristics for classification of different types of exosomes (Fig. 1). Using the CNN, researchers can process a large amount of data with less time and cost.

2. Materials and Methods

2.1. *Chemicals and instruments*

Tetrachloroauric (III) acid hydrate ($AuCl_3 \cdot HCl \cdot 4H_2O$) was purchased from China National Medicines Co.,

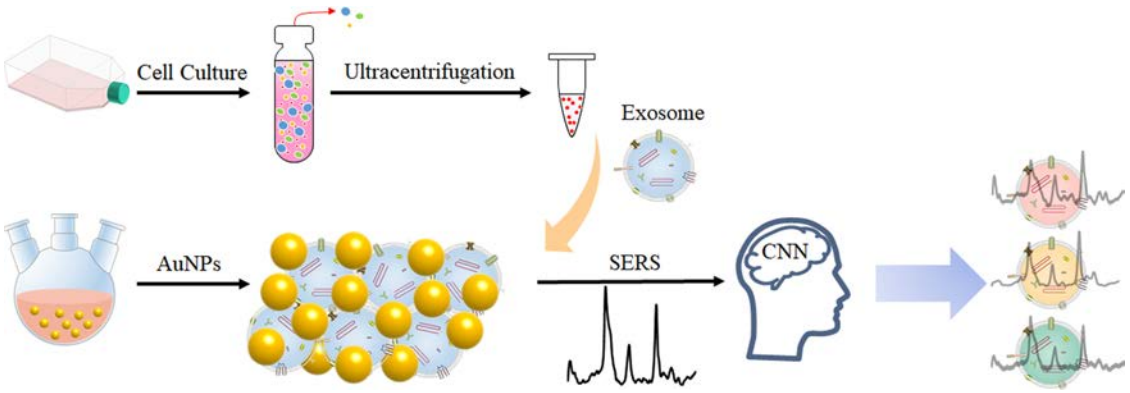

Fig. 1. Schematic illustration a method of SERS combined with CNN to detect exosomes from normal and breast cancer cells. (The golden spheres represent AuNPs, the blue vesicle-like spheres represent exosomes, and the red, yellow and green vesicle-like spheres represent exosomes derived from different cells.)

Ltd, sodium citrate and Phosphor-tungstic acid was obtained from Aladdin (Shanghai, China), the human breast cancer cell lines MCF-7 and MDA-MB-231 were purchased from Cell Bank of the Chinese Academy of Sciences, the human normal breast epithelial cell line MCF-10A were purchased from Procell Life Science & Technology Co., Ltd.

Dulbecco's modified eagle medium (DMEM), fetal bovine serum (FBS), trypsin and penicillin-streptomycin were provided by Beyotime Biotechnology (Shanghai, China). All other reagents used in this text as received did not need any purification.

Beckman Optima L-100XP ultracentrifuge, JEOL JEM-1400 PLUS 120 kV transmission electron microscope, Malvern Nanosight ns 300, *inVia* confocal Raman microscopy system (*Renishaw*, England).

2.2. *Cell culture*

The cryopreserved cell strains taken out of the −80°C refrigerator were quickly thawed and recovered in a 37°C-water bath, and then cultured in a 37°C, 5% CO_2 incubator. Change the culture medium according to the cleanliness and color of the culture medium. When the cells have grown to about 70–80%, the cells are passaged.

2.3. *Synthesis of SERS substrate-gold nanospheres*

Pour the 100 mL mass fraction of 0.01% chloroauric acid solution into a round bottom flask, stir and heat until the solution boils and continue for 2 min, add 4 mL mass fraction of 1% sodium citrate solution, continue to react for 10 min until the color of the synthesis solution no longer changes, stop heating and continue stirring. After the synthesis solution has cooled to room temperature, store it in a refrigerator at 4°C for characterization and application.[46]

2.4. *Exosome separation*

Based on the gold method of exosome extraction–ultracentrifugation,[47] we improved this method, the detail operation is as follows: When the cells grow in T225 culture flask to more than 80% (depending on the cell growth rate), remove the medium with serum and wash for 2–3 times with PBS, then replace with 80 mL serum-free medium (basic medium) and incubate for 24 h. The extraction process of exosomes was carried out at 4°C. Collect the cell culture supernatant and transfer it to a 50 mL centrifuge tube, then centrifuge at 500 g for 10 min. Remove the precipitate (removing non-adherent cells) and transfer the supernatant to a new centrifuge tube with a centrifugal force of 2000 g for 10 min. Remove the precipitate (removing dead cells) and transfer the supernatant to a new high-speed centrifuge tube, setting centrifuge force at 10,000 g and run for 20 min (Removing cell debris). Remove the precipitate, filter the supernatant with a 0.22 μm microfilter (removing cell debris). Transfer the filtrate to a 39 mL ultra-isolation tube and balance it at the thousandth position and use a fixed-angle rotor and ultracentrifuge at 120,000 × g centrifugal force for 90 min. Remove supernatant, resuspend the precipitate obtained by centrifugation in physiological saline, then transfer resuspension to a 6.5 mL ultra-isolation tube with

120,000 × g ultracentrifugation for 90 min, remove the supernatant, and resuspend the exosomes in 200 μL physiological saline and stored in −80°C refrigerator for use. When the cell culture supernatant obtained by low-speed centrifugation is insufficient, use physiological saline to supplement the balance.

2.5. *Identification of exosomes*

2.5.1. *Transmission electron microscope*

After fixing the copper mesh with tweezers, add 1 drop of exosomal solution, settling for 10 min, suck the liquid away from the edge with filter paper and use 1 drop of 1% phosphotungstic acid for negative staining for 1 min. The filter paper was blotted dry, then mixed the phosphotungstic acid and the sample in ratio of 1:1. Rinse the copper mesh three times, the shape and size of exosomes were observed under 120 kV TEM after baking or drying at room temperature.

2.5.2. *Nanoparticle tracking analysis*

The concentration and particle size of exosomes after ultracentrifugation were acquired by nanoparticle tracking analysis (NTA) (Malvern Nanosight NS300). The exosomes after centrifugation were diluted and put 1 mL into the sample pool. The instrument and various measurement parameters were adjusted to obtain the average particle size of the sample and the concentration of the original solution.

2.6. *Exosome detection by the SERS method*

In this experiment, *Renishaw inVia* confocal Raman microscopy system was used to acquire the SERS data. After power on, calibration and focusing, drop mixture of 10 μL exosomal solution with 2 μL AuNPs evenly on the silicon wafer. The SERS signal is acquired immediately when the liquid is dried. The emission wavelength of the laser is 785 nm with power of 0.5 mW to prevent excessive power burns the sample. The microscope is a Leica DM2500 with 50× objective lens magnification. The spectral range of Raman signal is 600–1800 cm^{-1}, and the exposure time is 4 s. After collecting the exosomes of each cell three times, the exosomes were detected by *inVia* confocal Raman microscopy system. About 130 locations are randomly detected (The distance between two adjacent points is greater than 200 nm), and the SERS spectral data of each location is obtained from the averaged spectral of three spectral lines. All spectra are acquired under the same conditions. Before data qualitative analysis, Vancouver Raman spectrum processing software was utilized to perform spectra baseline correction and fluorescence background subtraction.

2.7. *Neural network structure*

The network structure is illustrated in Fig. 2. The framework was organized with an initial convolutional layer, followed by a batch normalized (BN) layer, a rectified (Relu) layer, a pooling layer, eight serial basic block, a fully connected layer and a softmax output layer. The basic block consists of serials of convolutions, BN and Relu. There is a dropout layer between four blocks. For ternary classification, the exosomes of each cell were labeled with 0, 1 and 2.

2.7.1. *Model training and verification*

We trained and tested the network with a data set of exosomes SERS spectra, divided into 70%

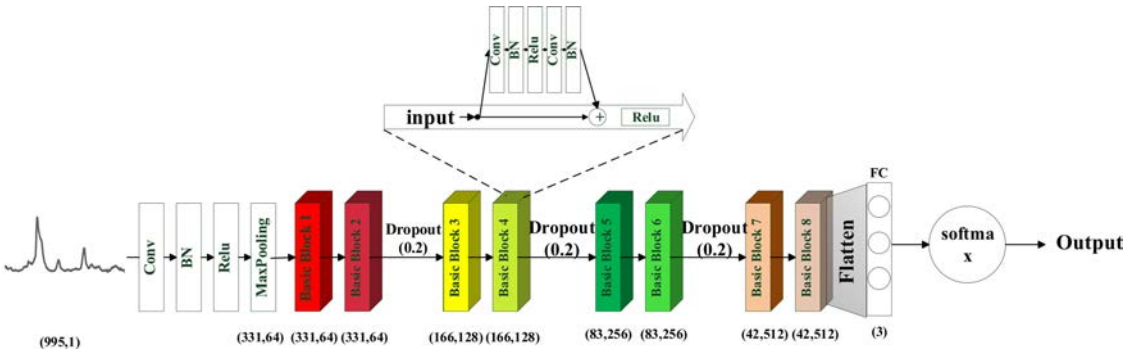

Fig. 2. Architecture of the resnet-based deep learning model.

training, 10% validation and 20% testing. Using the Adam algorithm,[37] a stochastic gradient-based optimizer, with an initial learning rate $1e^{-7}$ to train our network. The training process will also stop when loss stop declines. We implemented the network in Python 3.6 with Keras (Tensorflow-backend) on a PC with an Intel i7 CPU.

3. Result

3.1. *Characterization of synthetic gold nanoparticles (AuNPs)*

The synthesized AuNPs solution was translucent red (Fig. 3(a)). The synthesis solution was scanned by UV-VIS absorption spectrum in the wavelength range of 450–1000 nm. In Fig. 3(a), the width of the main peak is small, and the maximum absorption peak wavelength of the synthetic solution is $\lambda_{max} = 519$ nm, with the maximum absorbance $Abs_{max} = 0.1756$. From Fig. 3(b), it can be found that the diameter of the AuNPs was uniform and the diameter was about 16 nm, which was consistent with the absorption peak of the gold nanoparticles. The relationship between the extreme wavelength and the particle diameter can confirm that the synthetic liquid is AuNPs.[48]

3.2. *The characterization of exosomes*

Under the TEM, the exosomes secreted by the cell lines can be observed clearly, which are a classic saucer-shaped with a particle size of about 50–200 nm. A double membrane-like structure can be seen at the edge of exosomal vesicles with clear background and less pollutants, and the exosomes can also be seen clustered together (Figs. 4(a)–4(c)), these results are in accordance with before report.[47]

To research the particle size of exosomes, NTA method was employed in this experiment. It is shown in Fig. 4(d) that the average diameter of exosomes of MCF-7 is 73.4 nm, and the main peak diameter of the particle size is 73.5 nm. From Fig. 4(e), the diameters of most exosomes of MDA-MB-231 are distributed between 70–160 nm, the average particle size is 109.5 nm, and the main peak diameter of particle size is 75.5 nm. From Fig. 4(f), it can be found that the diameter of most MCF-10A exosomes distributes between 30–70 nm, the average particle size is 51.6 nm and the main peak diameter of particle size is 54.5 nm.

3.3. *Raman spectroscopy detection*

To study the AuNPs enhancement effects on the exosomes Raman scattering, the Raman spectra and SERS spectra of MDA-MB-231 exosomes are detected. From Figs. 5(a) and 5(b), it can be seen that only a few Raman peaks could be observed in the exosomes without adding AuNPs because almost all of the Raman signals are masked by the large fluorescence background. But in the spectra of exosomes added with AuNPs, the intensity of many dominant vibration bands increased dramatically. It indicates that there is a strong interaction between the AuNPs and exosomes.

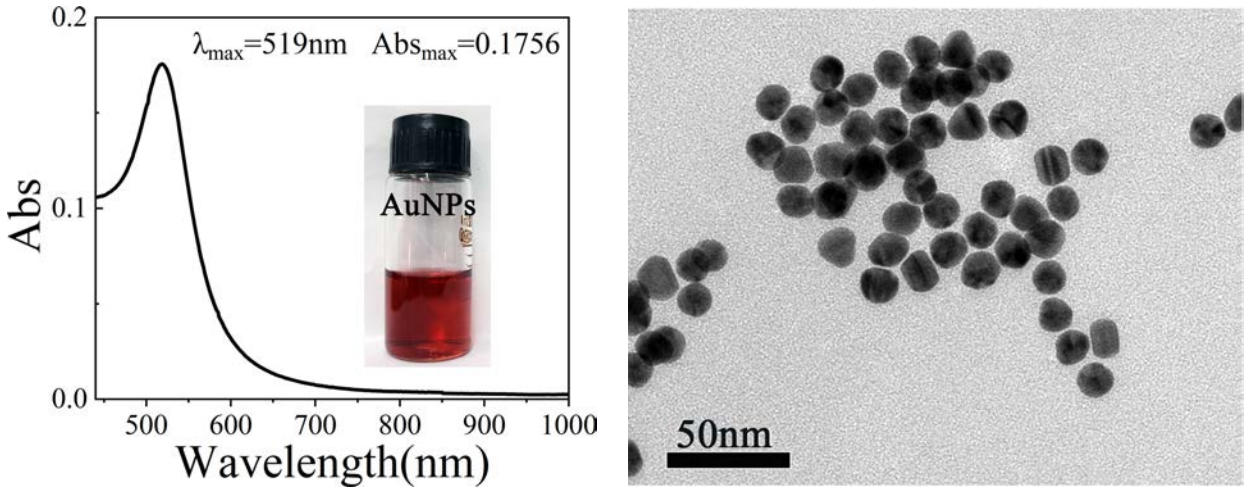

(a) (b)

Fig. 3. (a) Ultraviolet-visible absorption spectrogram (The translucent red is synthesized AuNPs.) and (b) TEM of the AuNPs.

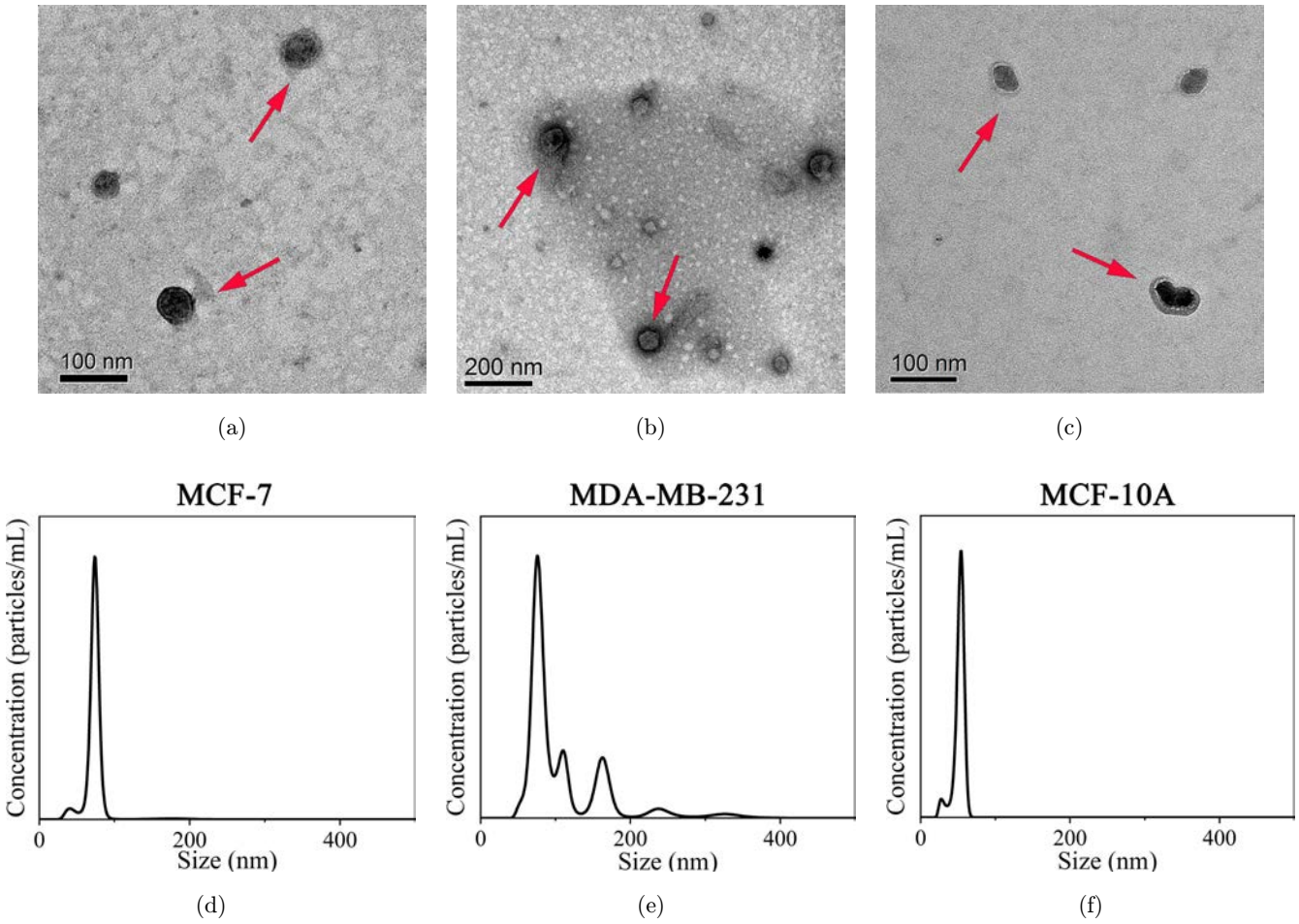

Fig. 4. The characterization of exosomes. (a), (b) and (c) are the exosomes TEM images of MCF-7, MDA-MB-231 and MCF-10A, respectively. (d), (e) and (f) are the exosomes size distribution and concentration relationship curves of MCF-7, MDA-MB-231 and MCF-10A, respectively.

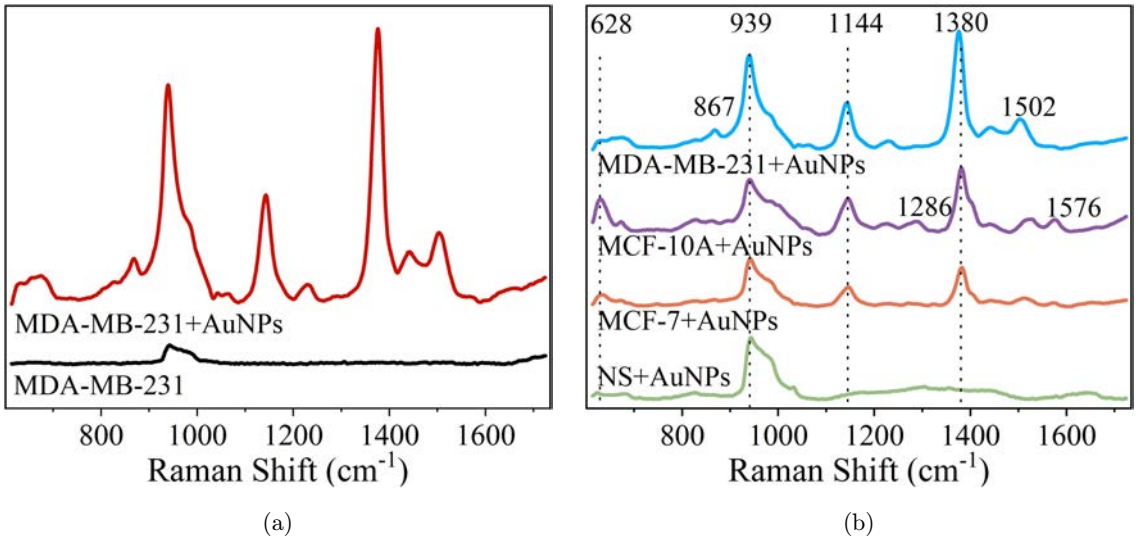

Fig. 5. SERS characteristic spectrum of exosomes. (a) Comparison of exosomes of MDA-MB-231 cells with or without AuNPs, adding AuNPs to enhance the Raman signal of exosomes. (b) Three exosomes enhanced by SERS and normal saline (NS) without exosomes under the same conditions Raman signal comparison.

Table 1. Comparison and preliminary attribution of SERS peaks of exosomes from different cell sources and references.

Raman Shift/cm^{-1} (Reference data in parentheses)			
MCF-7	MDA-MB-231	MCF-10A	Assignments
631(627)	625(629)	630(636)	Deformation vibration of adenine ring, phenylalanine C–C torsional vibration
	654(658)		Tyrosine vibration, Guanine
736(735)	736(735)	736(735)	Adenine
826(828)	825(826)	830(822)	Sugar–phosphate backbone vibration, protein, C–O–O vibration typical of phospholipids
867(855)	867(870)	864(854)	Cholesterol, oxyproline, tryptophan, glycogen, C–C stretch proline ring in collagen
939(920)	939(921)	939(919)	C=C stretching vibration, proline
none (999)	none (998)	999(998)	symmetric respiratory vibration of phenylalanine
1145(1150)	1142(none)	1145(1143)	CH vibration in protein, ribose–phosphate
	1229(none)	1223(1221)	Amide III
		1286 (1264)	Amide III (e.g., protein), C=C (e.g., fatty acids)
1380(1376)	1376(1376)	1380(1374)	Carbohydrate, adenine, guanine, thymine
1510(none)	1502(none)	1531(1532)	Vibration of (–C=C–) conjugated
1571(1581)	none (1580)	1576(1573)	Guanine, adenine, purine, phenylalanine, tyrosine

Note: Reference data and attribution of SERS peaks in the table cited from the literature.[50]

To distinguish the SERS spectra of MCF-7, MDA-MB-231 and MCF-10A exosomes, the SERS spectra were averaged, basal removed, and smoothed after measuring. From Fig. 5(b), it can be seen that the exosomes of different cells had similar peaks, which were difficult to differentiate. The common Raman peaks are near 939, 1145 and 1380 cm^{-1}, corresponding to the proline C=C stretching vibration, the CH vibration of the protein, ribosome–phosphate and Carbohydrates and nucleotides (adenine, guanine, thymine), respectively. But there is a little bit difference such as at peaks of 1286 cm^{-1}, and 1575 cm^{-1}, etc. The intensity of cancer cell lines (MCF-7 and MDA-MB-231) is lower than that of normal cell line (MCF-10A), which are corresponding of the lipids, proteins and carbohydrates. Recently, some researchers have proved that diploid, triploid, binuclear or multinucleated cells may appear in the process of cancer cell proliferation.[49] Disorders in the composition and metabolism of nucleic acid and protein make cancer cells have the ability to proliferate indefinitely, so the nucleic acid content of cancer cells is higher than that of normal cells. Since cancer cells secrete more exosomes and are rich in nucleic acids, including mRNA, microRNA and DNA, the Raman signal of nucleic acids in cancer-related exosomes is much stronger than that of normal exosomes. The metabolism of cancer cells is more active than normal cells, resulting in the consumption of more protein, lipids and energy-supply carbohydrates. It was also found that almost all of the Raman peaks are consistent with the documents (Table 1) (Reference data in parentheses and attribution of SERS peaks in the table cited from the literature Zhang *et al.*[50]), but this method wastes a lot of resources (money and time), and there will may be some errors. Therefore, this analysis method is difficult to implement, especially when analyzing large amounts of data.

3.4. *Convolutional neural network analysis*

To distinguish breast tumor cells from breast cells in exosomes in Raman spectrum, we used a CNN based on resnet.[37,51] 1160 SERS spectra were collected (400 spectra were collected from MCF-10A exosomes, 380 spectra from MDA-MB-231 exosomes and 380 spectra from MCF-7 exosomes.). The SERS signals were processed for baseline correction, denoising and min–max normalization. The final output scores of data from the three different exosomes (Figs. 6(a)–6(c)). The exosomes were undifferentiated at the initial 5 and 50 epochs; however, after 150 epochs they were well classified.

The loss and accuracy curves for training set, validation set, and test set are shown in Figs. 7(a)–7(c).

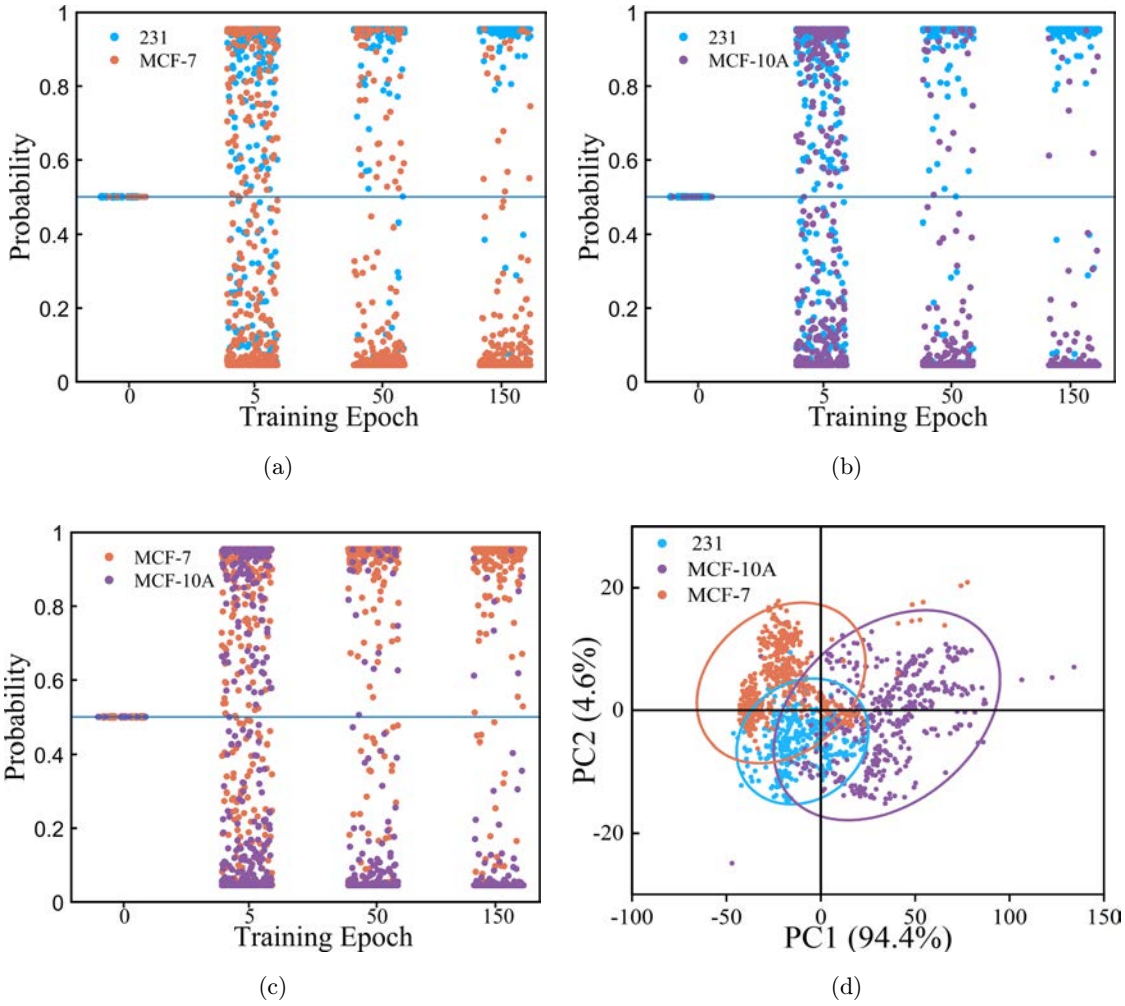

Fig. 6. Final output scores of representative data by training iterations. Cross-comparison of the exosomes from (a) MDA-MB-231 and MCF-7 cells; (b) MDA-MB-231 and MCF-10A cells; (c) MCF-7 and MCF-10A cells. (d) The PCA classification images of exosomes for MCF-7, MDA-MB-231 and MCF-10A.

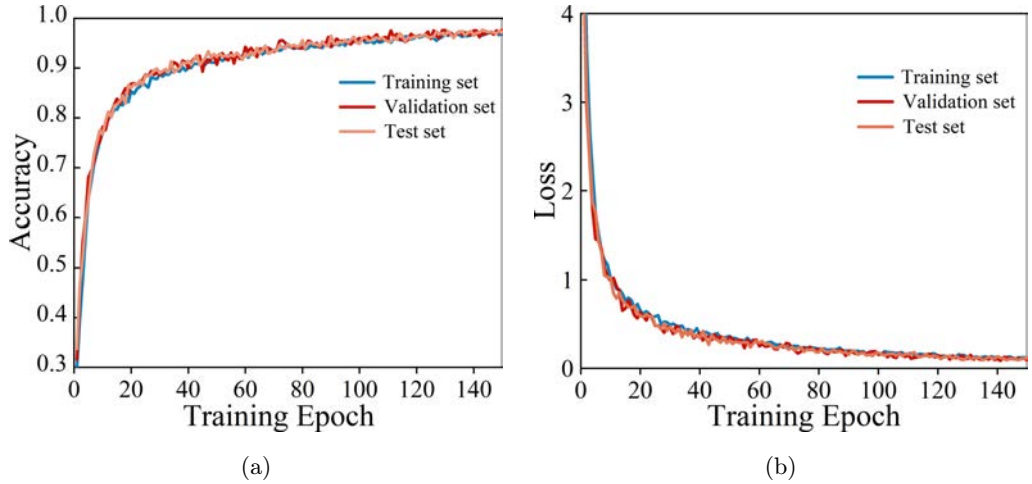

Fig. 7. Deep learning-based cell exosome classification. (a) Training, validation and test accuracy curves. (b) Training, validation and test loss curves. (c) ROC curves and their AUC values. (d) The confusion matrix.

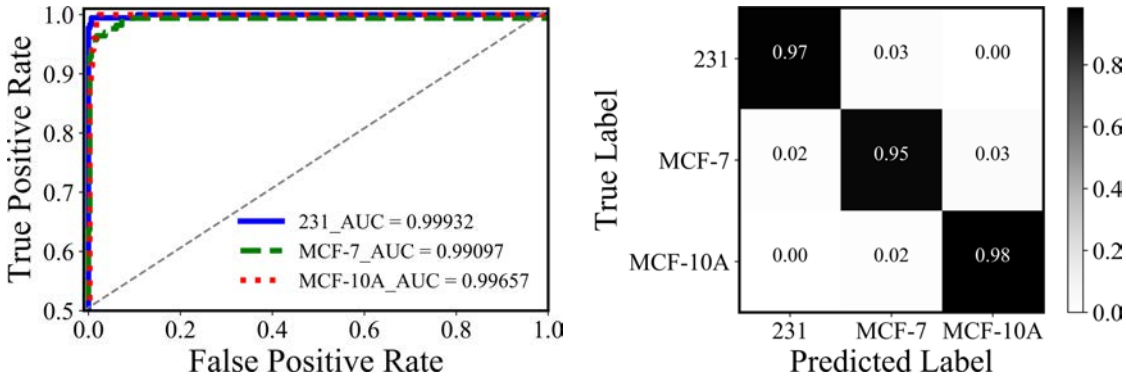

(c) (d)

Fig. 7. (*Continued*)

The model was constructed and the validated accuracy was measured to adjust the super parameter during the training process. Both the accuracy and loss curves tended to be stable. Our method achieved high accuracy with AUC of 0.999 for MDA-MB-231, and 0.991 for MCF-7, and 0.997 for MCF-10A (Fig. 7(c)). After a round of training, validation and test, all SERS spectral data containing three categories were classified. The results were summarized as the confusion matrix in Fig. 7(d). The value in the confusion matrix represents the ratio of the number of targets to the total number of samples. The results show that each category has only single-digit misclassification spectrum with an accuracy rate of more than 95%. In order to compare the classification performance of the traditional analysis, the PCA was used to classify the same SERS spectral data. From Fig. 6(d), the variance levels of PC1 and PC2 were 94.4% and 4.6%, respectively. The confidence ellipses of the three groups of exosomes overlap each other, and it is difficult to completely distinguish between cancer cells and normal cells. The sensitivity and specificity of SERS spectra for MDA-MB-231 and MCF-10A, MCF-7 and MCF-10A, MCF-7 and MDA-MB-231 were (81.2%, 56.3%), (89.7%, 80.8%), (67%, 66.1%), respectively.

4. Conclusion

In summary, this paper proves that the Resnet-based CNN structure is able to identify exosomes from different breast cancer cells and normal cells with high accuracy. The proposed method can detect the signal characteristics of exosome biomarkers extracted from label-free cell culture supernatant derived from mammary cells, and then classify them from normal breast cells or cancer cells according to their characteristics. Using this method, the experimenter can process the large amount of data collected in the experiment with less time and cost, and obtain stronger data analysis ability. Because this method has noninvasive, safe and sensitive advantages, which can be used to detect the exosome from breast cells in the blood, it may even become a regular tool of breast cancer screening, providing a new examination method for clinical liquid biopsy in the future.

Conflict of Interest

The authors declare that there are no conflict of interest related to this paper.

Acknowledgments

This work was supported by the National Natural Science Foundation of China (62175071, 11964032, 31300691, 32071399 and 61675072), the Science and Technology Project of Guangdong Province of China (2017A020215059), the Science and Technology Project of Guangzhou City (201904010323 and 2019050001) and the Innovation Project of Graduate School of South China Normal University (2019LKXM023).

Key Laboratory of OptoElectronic Science and Technology for Medicine of Ministry of Education (Fujian Normal University) (JYG2008). Xiao Ma and Honglian Xiong contributed equally to this work.

References

1. H. Sung, J. Ferlay, R. L. Siegel, M. Laversanne, I. Soerjomataram, A. Jemal, F. Bray, "Global

Cancer Statistics 2020: GLOBOCAN estimates of incidence and mortality worldwide for 36 cancers in 185 countries," *CA Cancer J. Clin.* **71**(3), 209–249 (2021).
2. A. Al Mannai, Y. Haik, A. Elmel, S. Qadri, K. M. Saud, "3D SERS-based biosensor for the selective detection of circulating cancer-derived exosomes," *Emergent Mater.* (2021), doi:https://doi.org/10.1007/s42247-021-00325-z.
3. U. Bick, R. M. Trimboli, A. Athanasiou, C. Balleyguier, P. A. T. Baltzer, M. Bernathova, K. Borbely, B. Brkljacic, L. A. Carbonaro, P. Clauser, E. Cassano, C. Colin, G. Esen, A. Evans, E. M. Fallenberg, M. H. Fuchsjaeger, F. J. Gilbert, T. H. Helbich, S. H. Heywang-Kobrunner, M. Herranz, K. Kinkel, F. Kilburn-Toppin, C. K. Kuhl, M. Lesaru, M. B. I. Lobbes, R. M. Mann, L. Martincich, P. Panizza, F. Pediconi, R. M. Pijnappel, K. Pinker, S. Schiaffino, T. Sella, I. Thomassin-Naggara, A. Tardivon, C. V. Ongeval, M. G. Wallis, S. Zackrisson, G. Forrai, J. C. Herrero, F. Sardanelli, W. L. R. B. E. D.-T. E. B. C. C. European Society of Breast Imaging, "Image-guided breast biopsy and localisation: Recommendations for information to women and referring physicians by the European Society of Breast Imaging," *Insights Imaging.* **11**(1), 12 (2020).
4. M. T. Mutar, M. M. Hameed, M. S. Goyani, A. S. Mahmood, A.-A. H. Obaid, Breast cancer screening, *Chapter 8 in Breast Cancer - Evolving Challenges and Next Frontiers*, M. T. Valarmathi, Eds., pp. 1–17, IntechOpen, London (2021).
5. K. B. Carreiro, J. P. G. D. Cunha, J. R. Filassi, C. Dinelli, Diagnostic, *Chapter 13 in Modern Breast Cancer Imaging*, S. J. Kim Hsieh, E. A. Morris, Eds., pp. 259–279, Springer, Cham (2022).
6. B. Secretan, C. Scoccianti, D. Loomis, L. B. Tallaa, V. Bouvard, F. Bianchini, K. Straif, "Breast-Cancer Screening — Viewpoint of the IARC Working Group," *N. Engl. J. Med.* **372**(24), 2353–2358 (2015).
7. F. J. Nassar, G. Chamandi, M. A. Tfaily, N. K. Zgheib, R. Nasr, "Peripheral blood-based biopsy for breast cancer risk prediction and early detection," *Front. Med. (Lausanne).* **7**, 28 (2020).
8. B.-T. Pan, K. Teng, C. Wu, M. Adam, R. M. Johnstone, "Electron microscopic evidence for externalization of the transferrin receptor in vesicular form in sheep reticulocytes," *J. Cell Biol.* **101**(3), 942–948 (1985).
9. C. Harding, P. Stahl, "Transferrin recycling in reticulocytes: pH and iron are important determinants of ligand binding and processing," *Biochem. Biophys. Res. Commun.* **113**(2), 650–658 (1983).
10. B. Pan, R. M. Johnstone, "Fate of the transferrin receptor during maturation of sheep reticulocytes *in vitro*: Selective externalization of the receptor," *Cell.* **33**(3), 967–978 (1983).
11. R. M. Johnstone, M. Adam, J. R. Hammond, L. Orr, C. Turbide, "Vesicle formation during reticulocyte maturation. Association of plasma membrane activities with released vesicles (exosomes)," *J. Biol. Chem.* **262**(19), 9412–9420 (1987).
12. C. V. Harding, J. E. Heuser, P. D. Stahl, "Receptor-mediated endocytosis of transferrin and recycling of the transferrin receptor in rat reticulocytes," *J. Cell Biol.* **97**(2), 329–339 (1983).
13. F. Khan, E. M. Saleh, H. Alawadhi, R. Harati, W. Zimmermann, R. Elawady, "Inhibition of exosome release by ketotifen enhances sensitivity of cancer cells to doxorubicin," *Cancer Biol. Ther.* **19**(1), 25–33 (2018).
14. J. Kowal, M. Tkach, C. Thery, "Biogenesis and secretion of exosomes," *Curr. Opin. Cell Biol.* **29**, 116–125 (2014).
15. S. S. Kanwar, C. J. Dunlay, D. M. Simeone, S. Nagrath, "Microfluidic device (ExoChip) for on-chip isolation, quantification and characterization of circulating exosomes," *Lab Chip.* **14**(11), 1891–1900 (2014).
16. X. Li, Z. Yang, "Regulatory effect of exosome on cell apoptosis," *J. Cent. South Univ. Med. Sci.* **42**(2), 215 (2017).
17. C. He, S. Zheng, Y. Luo, B. Wang, "Exosome theranostics: Biology and translational medicine," *Theranostics* **8**(1), 237–255 (2018).
18. W. Li, C. Li, T. Zhou, X. Liu, X. Liu, X. Li, D. Chen, "Role of exosomal proteins in cancer diagnosis," *Mol. Cancer.* **16**(1), 1–12 (2017).
19. Y. Li, C. Han, J. Wang, J. Zhou, C. Liang, K. Ranganna, Y. Song, "Exosomes mediate the beneficial effects of exercise," *Adv. Exp. Med. Biol.* **1000**, 333–353 (2017).
20. A. Lai, V. Kinhal, Z. Nuzhat, R. Menon, G. E. Rice, C. Salomon, "Proteomics method to identification of protein profiles in exosomes," *Methods Mol. Biol.* **1710**, 139–153 (2018).
21. S. A. Melo, C. Moutinho, S. Ropero, G. A. Calin, S. Rossi, R. Spizzo, A. F. Fernandez, V. Davalos, A. Villanueva, G. Montoya, H. Yamamoto, S. Schwartz, Jr., M. Esteller, "A genetic defect in exportin-5 traps precursor microRNAs in the nucleus of cancer cells," *Cancer Cell.* **18**(4), 303–315 (2010).
22. H. J. Oh, Y. Shin, S. Chung, D. W. Hwang, D. S. Lee, "Convective exosome-tracing microfluidics for analysis of cell-non-autonomous neurogenesis," *Biomaterials* **112**, 82–94 (2017).
23. A. Zhao, L. Guo, A. Chen, "Exosome in tumor: Diagnosis and therapy," *China Cancer* **26**(3), 190–195 (2017).
24. R. Kalluri, "The biology and function of exosomes in cancer," *J. Clin. Invest.* **126**(4), 1208–1215 (2016).

25. E. Anastasiadou, F. J. Slack, "Cancer. Malicious exosomes," *Science* **346**(6216), 1459–1460 (2014).
26. H. Shao, J. Chung, D. Issadore, "Diagnostic technologies for circulating tumour cells and exosomes," *Biosci. Rep.* **36**(1), e00292 (2016).
27. B. S. Chia, Y. P. Low, Q. Wang, P. Li, Z. Gao, "Advances in exosome quantification techniques," *TrAC Trends Anal. Chem.* **86**, 93–106 (2017).
28. C. V. Raman, K. S. Krishnan, "A new type of secondary radiation," *Nature* **121**(3048), 501–502 (1928).
29. K. Kneipp, H. Kneipp, I. Itzkan, R. R. Dasari, M. S. Feld, "Surface-enhanced Raman scattering and biophysics," *J. Phys. Condensed Matter.* **14**(18), R597 (2002).
30. H. Liu, X. Liu, L. Mo, C. Chen, H. Zhong, Z. Guo, Z. Liu, "Progress in the development and application of transitional technology of surface-enhanced Raman spectroscopy," *Colloids Interface Sci. Commun.* **43**, 100443 (2021).
31. M. Zhou, C. Liao, Z. Ren, H. Fan, J. Bai, "Bioimaging technologies based on surface-enhanced Raman spectroscopy and their applications," *Chin. J. Opt. Appl. Opt.* **6**, 633–642 (2013).
32. Y. Li, Y. X. Guo, B. G. Ye, Z. F. Zhuang, P. L. Lan, Y. Zhang, H. Q. Zhong, H. Liu, Z. Y. Guo, Z. M. Liu, "Rapid label-free SERS detection of foodborne pathogenic bacteria based on hafnium ditelluride-Au nanocomposites," *J. Innov. Opt. Heal. Sci.* **13**(5) 2041004 (2020).
33. M. Blanco-Formoso, R. A. Alvarez-Puebla, "Cancer diagnosis through SERS and other related techniques," *Int. J. Mol. Sci.* **21**(6), 2253 (2020).
34. L. Tirinato, F. Gentile, D. Di Mascolo, M. L. Coluccio, G. Das, C. Liberale, S. A. Pullano, G. Perozziello, M. Francardi, A. Accardo, F. De Angelis, P. Candeloro, E. Di Fabrizio, "SERS analysis on exosomes using super-hydrophobic surfaces," *Microelectron Eng.* **97**, 337–340 (2012).
35. C. Lee, R. P. Carney, S. Hazari, Z. J. Smith, A. Knudson, C. S. Robertson, K. S. Lam, S. Wachsmann-Hogiu, "3D plasmonic nanobowl platform for the study of exosomes in solution," *Nanoscale* **7**(20), 9290–9297 (2015).
36. S. Stremersch, M. Marro, B.-E. Pinchasik, P. Baatsen, A. Hendrix, S. C. De Smedt, P. Loza-Alvarez, A. G. Skirtach, K. Raemdonck, K. Braeckmans, "Identification of individual exosome-like vesicles by surface enhanced Raman spectroscopy," *Small* **12**(24), 3292–3301 (2016).
37. H. Shin, S. Oh, S. Hong, M. Kang, D. Kang, Y. G. Ji, B. H. Choi, K. W. Kang, H. Jeong, Y. Park, S. Hong, H. K. Kim, Y. Choi, "Early-stage lung cancer diagnosis by deep learning-based spectroscopic analysis of circulating exosomes," *ACS Nano* **14**(5), 5435–5444 (2020).
38. G. Li, N. Zhu, J. Zhou, K. Kang, X. Zhou, B. Ying, Q. Yi, Y. Wu, "A magnetic surface-enhanced Raman scattering platform for performing successive breast cancer exosome isolation and analysis," *J. Mater. Chem. B* **9**(11), 2709–2716 (2021).
39. D. Cheng, M. Liu, J. Fu, Y. Wang, Classification of MR brain images by combination of multi-CNNs for AD diagnosis, *Proc. SPIE 10420, Ninth Int. Conf. Digital Image Processing (ICDIP)*, Vol. 1042042, Hong Kong, China (2017).
40. J. Liu, M. Osadchy, L. Ashton, M. Foster, C. J. Solomon, S. J. Gibson, "Deep convolutional neural networks for Raman spectrum recognition: A unified solution," *Analyst* **142**(21), 4067–4074 (2017).
41. S. Berisha, M. Lotfollahi, J. Jahanipour, I. Gurcan, M. Walsh, R. Bhargava, H. Van Nguyen, D. Mayerich, "Deep learning for FTIR histology: Leveraging spatial and spectral features with convolutional neural networks," *Analyst* **144**(5), 1642–1653 (2019).
42. V. Zivanovic, S. Seifert, D. Drescher, P. Schrade, S. Werner, P. Guttmann, G. P. Szekeres, S. Bachmann, G. Schneider, C. Arenz, "Optical nanosensing of lipid accumulation due to enzyme inhibition in live cells," *ACS Nano* **13**(8), 9363–9375 (2019).
43. F. Lussier, D. Missirlis, J. P. Spatz, J.-F. Masson, "Machine-learning-driven surface-enhanced raman scattering optophysiology reveals multiplexed metabolite gradients near cells," *ACS Nano* **13**(2), 1403–1411 (2019).
44. R. M. Davis, B. Kiss, D. R. Trivedi, T. J. Metzner, J. C. Liao, S. S. Gambhir, "Surface-enhanced Raman scattering nanoparticles for multiplexed imaging of bladder cancer tissue permeability and molecular phenotype," *Acs Nano* **12**(10), 9669–9679 (2018).
45. Y. Li, Z. Hao, H. Lei, "Survey of convolutional neural network," *J. Comput. Appl.* **36**(9), 2508–2515, 2565 (2016).
46. R. Zhou, D. Fu, D. Yuan, Y. Wu, K. Qiao, "Preparation, characterization and application of gold nanoparticles," *J. Sichuan Univ. Sci. Eng. (Nat. Sci. Edn.).* **29**(3), 14–18 (2016).
47. P. Li, M. Kaslan, S. H. Lee, J. Yao, Z. Gao, "Progress in exosome isolation techniques," *Theranostics* **7**(3), 789–804 (2017).
48. X. Li, Z. Yang, H. Zhou, "Studying the absorption spectrum properties of the gold nanosphere—The effect of the size on the absorption spectra of the nanoparticles," *J. Zhangzhou Teachers College (Nat. Sci.)* **17**(2), 31–34 (2004).

49. J. L. Griffin, J. P. Shockcor, "Metabolic profiles of cancer cells," *Nat. Rev. Cancer* **4**(7), 551–561 (2004).
50. P. Zhang, L. Wang, Y. Fang, D. Zheng, T. Lin, H. Wang, "Label-free exosomal detection and classification in rapid discriminating different cancer types based on specific Raman phenotypes and multivariate statistical analysis," *Molecules* **24**(16), 2947 (2019).
51. K. He, X. Zhang, S. Ren, J. Sun, Deep residual learning for image recognition, *Proc. 2016 IEEE Conf. Computer Vision and Pattern Recognition (CVPR)*, pp. 770–778, Las Vegas, NV, USA (2016).